Wideband Modeling of Arbitrarily Shaped E-Plane Waveguide Components by the "Boundary Integral–Resonant Mode Expansion Method"

Paolo Arcioni, *Member, IEEE*, Marco Bressan, *Member, IEEE*, Giuseppe Conciauro, *Member, IEEE*, and Luca Perregrini

***Abstract*— The boundary integral–resonant mode expansion method is used for the solution of the eigenvalue problem involved in the determination of the poles and the residues of the Y-parameters of arbitrarily shaped E-plane waveguide junctions. Using this method, the frequency response and its sensitivity to deformations of the boundary can be calculated much faster than by other more conventional methods for arbitrary shapes. Therefore, the described algorithm is eligible for setting up very efficient CAD tools to produce optimized designs of complex E-plane components in reasonable times. Some examples demonstrate the efficiency of the method in the modeling of components of practical interest.**

I. Introduction

WAVEGUIDE components of unusual shapes are often attractive to fulfill many design requirements, such as small-size or high-power capability. Anyway, the choice of possible shapes is limited by the fact that the available CAD tools either are restricted to structures that can be segmented into parts of very simple geometry or are not fast enough to obtain optimized designs in reasonable times.

In a recent paper [1], we presented a very efficient field-theoretical method for the wideband modeling of arbitrarily shaped H-plane junctions among rectangular waveguides. This method has the distinguishing feature of yielding the Y-parameters in the form of a pole expansion in the frequency domain. It is based on the solution of a 2D eigenvalue problem carried-out by the "Boundary Integral–Resonant Mode Expansion (BI–RME) Method," a denomination recently introduced to indicate a general procedure to solve different eigenvalue problems arising in electromagnetic theory [1]–[6]. Though the eigenvalue problem could be solved by standard methods (e.g., the FEM), the use of the BI–RME method results in a much shorter computing time, thus allowing a very fast modeling of H-plane components. This paper describes the extension of the BI–RME method to the case of E-plane components. This extension is not trivial since it entails some theoretical complications, due to the different boundary condition.

As in the case of H-plane components, the BI–RME method yields—with a negligible computational effort—the variations of the poles and the residues of the Y-parameters caused by small deformations of the side walls. This possibility, together with the intrinsic rapidity of the algorithm, can be exploited to implement fast optimization procedures or to set mechanical tolerances.

Incidentally, the eigenvalue problem considered in this work is identical to that encountered in the determination of the TE modes of a waveguide, a problem which has already been treated in its vector form by an algorithm similar to the one described in this paper [3]. Here, this problem is treated in scalar form by a more efficient algorithm, which avoids some spurious solutions at nominally zero frequency that affected the previous version of the algorithm.

Manuscript received February 26, 1996; revised July 22, 1996. This work was supported by MURST.

The authors are with the Department of Electronics of the University of Pavia, I-27100 Pavia, Italy.

Publisher Item Identifier S 0018-9480(96)07907-0.

II. Theory

A. Wideband Representation of the Admittance Parameters

Let us consider an arbitrary lossless E-plane component containing a homogeneous, isotropic, nondispersive medium, whose permittivities are ϵ, μ (Fig. 1). We have N terminal waveguides of width W, operating in the dominant TE_{10} mode. The cross-section of the structure is denoted by S, the height and the length of the nth waveguide by H_n and L_n, respectively. We assume

$$L_n \geq W. \tag{1}$$

By the same argument presented in [1] we can show that under this assumption the Y-parameters can be approximated by the pole expansion

$$Y_{mn}(\omega) \approx \frac{\pi\delta_{mn}}{jk\eta W} + \frac{jkW\delta_{mn}}{2\pi\eta} + \frac{jk^3}{\eta}\sum_i \frac{c_{mi}c_{ni}}{\kappa_i^2(\kappa_i^2 - k^2)} \tag{2}$$

where $m, n = 1, 2, \cdots, N$; δ_{mn} is the Kronecker index; η is the characteristic impedance of the medium; $k = \omega\sqrt{\epsilon\mu}$ is the wavenumber at the frequency ω; κ_i is the resonating wavenumber of the ith mode of the cavity obtained short-circuiting the ports; the c-coefficients are given by

$$c_{ni} = \int_{A_n} \vec{h}_n \cdot \vec{\mathcal{H}}_i \, dA_n \tag{3}$$

where A_n is the surface of the nth port, $\vec{h}_n$ is the magnetic vector of the TE_{10} mode of the nth waveguide and $\vec{\mathcal{H}}_i$ is the

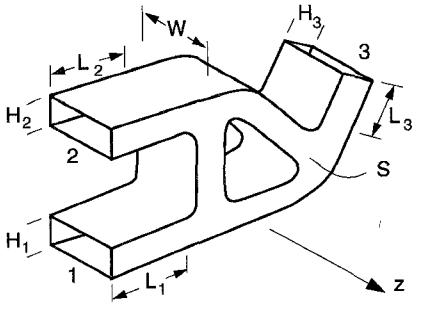

Fig. 1. An E-plane multiport waveguide component.

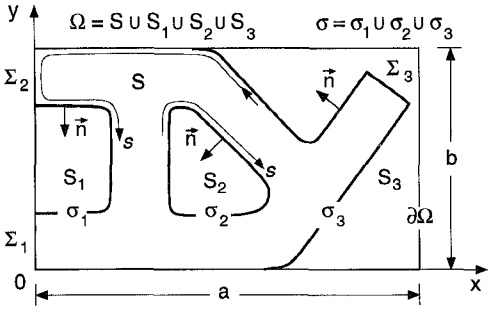

Fig. 2. The cross-section of the component of Fig. 1 embedded in the rectangular domain Ω. The ports Σ_1, Σ_2, Σ_3 are closed by electric walls.

magnetic vector of the ith resonant mode of the cavity. Both $\vec{\mathcal{H}}_i$ and $\vec{h}_n$ are normalized to one in the cavity volume and in A_n, respectively.

As discussed in [1], the approximation (2) is acceptable if k does not exceed the value $k_{\max}$ of the wavenumber at the maximum operating frequency of the waveguides. Furthermore, the approximation is more accurate the longer the terminal waveguides are, and it is adequate for most practical purposes, even for the minimum lengths allowed by (1).

The only cavity modes that are coupled to the TE_{10} mode of the waveguides are the TE-to-z resonant modes that depend on z by the factor $\sin(\pi z/W)$. Representing the magnetic vector of the cavity modes by a Hertz potential of the type $\psi(x, y)\sin(\pi z/W)$ and introducing the expression of $\vec{h}_n$, we easily find

$$c_{ni} = \frac{1}{\chi_i \kappa_i \sqrt{H_n}} \int_{\Sigma_n} \nabla^2 \psi_i \, ds \tag{4}$$

where s (see Fig. 2) denotes a coordinate taken on ∂S; the integration is performed over the segment Σ_n corresponding to the nth port; χ_i and ψ_i are the ith eigenvalue and eigenfunction of the equation

$$\nabla^2 \psi + \chi^2 \psi = 0 \quad (\chi \neq 0) \quad \text{in } S \tag{5}$$

$$\frac{\partial \psi}{\partial n} = 0 \quad \text{on } \partial S \tag{6}$$

$$\int_S \psi^2 \, dS = 1 \tag{7}$$

and the resonating wavenumber κ_i is given by

$$\kappa_i = \sqrt{\chi_i^2 + \left(\frac{\pi}{W}\right)^2}. \tag{8}$$

The eigenfunctions are continuously differentiable to all orders inside S. On the boundary, $\partial\psi/\partial s$ may diverge at the reentrant edges of S.

The basic problem to be solved for modeling a particular structure by (2) is the determination of a sufficient number of the lowest-order eigensolutions of (5). Note that this problem is identical to that encountered in the determination of the TE modes of a waveguide of cross-section S.

B. Integro-Differential Formulation of the Eigenvalue Problem

The domain of ψ is extended from S to a fictitious rectangular domain Ω including S (Fig. 2) and the original eigenvalue problem is replaced by the "enlarged problem"

$$\nabla^2 \psi + \chi^2 \psi = 0 \quad \chi \neq 0 \quad \text{in } \Omega^\dagger \tag{9}$$

$$\frac{\partial \psi}{\partial n} = 0 \quad \text{on } \sigma \text{ and } \partial\Omega \tag{10}$$

$$||\psi||_\Omega = 1 \tag{11}$$

where $\sigma = \sigma_1 \cup \sigma_2 \cup \cdots \cup \sigma_K$ is the part of ∂S not coincident with $\partial\Omega$; $\Omega^\dagger$ represents the domain Ω deprived of σ; and $||.||_\Omega$ denotes the norm of the real space $\mathcal{L}_2(\Omega)$. The enlarged problem is equivalent to the joint formulation of (5)–(7) and of the analogous problems for the domains $S_1, S_2, \cdots, S_K$ (see Fig. 2). Therefore, it admits two classes of solutions: the "internal" ones, that correspond to the eigensolutions of (5)–(7) in S and are zero in $S_1, S_2, \cdots, S_K$; the "external" ones, that differ from zero in one of the regions S_k and are zero elsewhere. Since both classes of solutions differ from zero in one region only, their normalization in Ω is equivalent to the normalization in that region. In spite of the presence of the useless external solutions, considering the enlarged problem rather than the original one is convenient, because it can be solved by the BI–RME method.

Using the divergence theorem, it is easily shown that (9)–(11) imply

$$\overline{\psi} = 0 \tag{12}$$

where the overline denotes the mean value in Ω. Furthermore, both the internal and the external solutions are continuously differentiable to any order in $\Omega^\dagger$, discontinuous at σ and, due to (10), with a continuous normal derivative. Therefore, by denoting quantities taken on the external and internal side of σ with the superscripts + and −, we have

$$\psi^+ - \psi^- = -f(s) \tag{13}$$

$$\frac{\partial \psi^+}{\partial n} - \frac{\partial \psi^-}{\partial n} = 0 \tag{14}$$

$$\nabla^2 \psi^+ - \nabla^2 \psi^- = \chi^2 f(s) \tag{15}$$

where s is taken on σ and f is some function representing the discontinuity of ψ. Note that, due to the singularity of $\partial\psi^\pm/\partial s$, this function varies very rapidly in the proximity of the points where the tangent to σ changes abruptly.

TABLE I
GREEN'S FUNCTIONS

$$G = \frac{1}{4\pi}\sum_{m=-\infty}^{\infty}(-1)^m \ln\frac{T_m^+}{T_m^-} \qquad F_0 = \frac{a}{3b} + \frac{x^2+x'^2}{2ab} - \frac{x+x'+|x-x'|}{2b} - \frac{1}{4\pi}\sum_{m=-\infty}^{\infty}\ln\left(4T_m^+T_m^-e^{-2|X_m|}\right)$$

$$\frac{\partial^2 F_1}{\partial x\partial x'} = \frac{x+x'-|x-x'|}{2b} - \frac{xx'}{ab} - \frac{1}{8\pi}\sum_{m=-\infty}^{\infty}(-1)^m\left[\ln\left(4T_m^+T_m^-e^{-2|X_m|}\right) + |X_m|\left(\frac{\cos Y^+ - e^{-|X_m|}}{T_m^+} + \frac{\cos Y^- - e^{-|X_m|}}{T_m^-}\right)\right]$$

$$\frac{\partial^2 F_1}{\partial x\partial y'} = \frac{1}{8\pi}\sum_{m=-\infty}^{\infty}X_m\left(\frac{\sin Y^+}{T_m^+} - \frac{\sin Y^-}{T_m^-}\right) \qquad \frac{\partial^2 F_1}{\partial y\partial x'} = -\frac{1}{8\pi}\sum_{m=-\infty}^{\infty}(-1)^m X_m\left(\frac{\sin Y^+}{T_m^+} + \frac{\sin Y^-}{T_m^-}\right)$$

$$\frac{\partial^2 F_1}{\partial y\partial y'} = \frac{1}{8\pi}\sum_{m=-\infty}^{\infty}\left[\ln\frac{T_m^+}{T_m^-} - |X_m|\left(\frac{\cos Y^+ - e^{-|X_m|}}{T_m^+} - \frac{\cos Y^- - e^{-|X_m|}}{T_m^-}\right)\right]$$

where: $X_m = \frac{\pi}{b}\left[x - (m+\frac{1}{2})a - (-1)^m(x' - \frac{a}{2})\right]$ $\qquad Y^{\pm} = \frac{\pi}{b}(y \pm y')$ $\qquad T_m^{\pm} = \cosh X_m - \cos Y^{\pm}$

x, y and x', y' are the coordinates of the observation and the source points, respectively

a and b are the lengths of the sides of Ω. The series converge more rapidly if $a > b$.

As discussed below, all the said features of the solutions are included in the following representation of ψ

$$\psi = \underbrace{-\int_\sigma \frac{\partial F_0(x, y; s')}{\partial n'} f(s')\, ds'}_{U_0} + \chi^2\left[\phi - \underbrace{\int_\sigma \frac{\partial F_1(x, y; s')}{\partial n'} f(s')\, ds'}_{U_1}\right] \tag{16}$$

where ϕ represents a zero-mean function, satisfying the Neumann boundary condition on $\partial\Omega$, continuously differentiable to all orders in $\Omega^\dagger$ and to the second order, at least, on σ; F_0 and F_1 are the Green's functions that satisfy

$$\nabla^2 F_0 = -\delta(x-x')\delta(y-y') + \frac{1}{ab} \tag{17}$$

$$\nabla^2 F_1 = -F_0 \tag{18}$$

$$\frac{\partial F_0}{\partial n} = \frac{\partial F_1}{\partial n} = 0 \text{ on } \partial\Omega$$

$$\overline{F_0} = \overline{F_1} = 0. \tag{19}$$

In (16), the notation used for the normal derivatives indicates they are taken with respect to the coordinates of the source point, that is placed on σ at the coordinate s'.

The representation (16) fulfills the requirement (12) because ϕ and the Green's functions have zero mean. It satisfies (13) and (14) because the integral denoted by U_0 represents the harmonic potential generated by a "double layer" of density f located on σ and because the other integral (which satisfies $\nabla^2 U_1 = -U_0$) is continuously differentiable to the first order. Furthermore, (15) is verified as well, because

$$\nabla^2\psi = \chi^2(U_0 + \nabla^2\phi) \tag{20}$$

where $\nabla^2\phi$ is continuous and $\chi^2 U_0$ has the right discontinuity.

Equations (9) and (10) are converted into two integro-differential equations, substituting (16), (20), and using the identity (see Appendix A)

$$\frac{\partial U_0}{\partial n} = \frac{\partial}{\partial s}\int_\sigma G(s, s')\frac{\partial f(s')}{\partial s'}\, ds' \tag{21}$$

where G satisfies

$$\nabla^2 G = -\delta(x-x')\delta(y-y') \tag{22}$$

$$G = 0 \quad \text{on } \partial\Omega \tag{23}$$

We obtain

$$\nabla^2\phi + \chi^2\left[\phi - \int_\sigma \frac{\partial F_1(x, y; s')}{\partial n'} f(s')\, ds'\right] = 0 \quad \text{in } \Omega \tag{24}$$

$$-\frac{\partial}{\partial s}\int_\sigma G(s, s')\frac{\partial f(s')}{\partial s'}\, ds' + \chi^2\left[\frac{\partial\phi}{\partial n} - \int_\sigma \frac{\partial^2 F_1(s, s')}{\partial n\,\partial n'} f(s')\, ds'\right] = 0 \quad \text{on } \sigma \tag{25}$$

The Green's functions F_0, F_1, G can be easily found in the form of eigenfunction expansions (see Appendix A). The expansions of F_0 and G can be converted into rapidly convergent one-index series. The same transformation—which is impossible for F_1—can be performed for the components of the dyadic $\nabla\nabla' F_1$, from which we obtain $\partial^2 F_1/\partial n\,\partial n' = \vec{n}\cdot\nabla\nabla' F_1\cdot\vec{n}'$. These series are reported in Table I. Note that the terms with $m = 0$ include the logarithmic singularities of the Green's functions.

The solution of the integro-differential equations (24) and (25) constitutes a linear eigenvalue problem in the unknown functions f and ϕ. Adding the specification $\chi \neq 0$ [see (9)] is necessary, because it is evident that the said equations are verified identically by spurious solutions with $\chi = 0$, $\phi = 0$, and f constant on each line $\sigma_1, \sigma_2, \cdots, \sigma_K$.

Furthermore, the normalizing condition (11) requires (see Appendix B)

$$\int_\sigma \int_\sigma G(s, s') \frac{\partial f(s)}{\partial s} \frac{\partial f(s')}{\partial s'} \, ds \, ds' + \int_\Omega |\nabla \nabla^2 \phi|^2 \, d\Omega = \chi^2. \tag{26}$$

C. BI–RME Representation of ψ and $\nabla^2 \psi$

We can represent ϕ and $\nabla^2 \phi$ by the Fourier series

$$\phi = \sum_{p,q} a_{pq} \Phi_{pq} \tag{27}$$

$$\nabla^2 \phi = -\sum_{p,q} a_{pq} \lambda_{pq}^2 \Phi_{pq} \tag{28}$$

where the a_{pq} are unknown coefficients and

$$\Phi_{pq} = \sqrt{\frac{2 - \delta_{0p} - \delta_{0q}}{ab}} \cos \frac{p\pi x}{a} \cos \frac{q\pi y}{b} \tag{29}$$

$$\lambda_{pq} = \sqrt{\left(\frac{p\pi}{a}\right)^2 + \left(\frac{q\pi}{b}\right)^2} \tag{30}$$

$$p, q = 0, 1, \cdots; \quad (p, q) \neq (0, 0). \tag{31}$$

The series converge uniformly due to the continuity of ϕ and $\nabla^2 \phi$.

It is noted that Φ_{pq} and λ_{pq} are related to the resonant modes of the rectangular box of cross-section Ω in the same way as the eigensolutions of (5)–(7) are related to the resonant modes of the short-circuited structure. For this reason, (27) is the "resonant mode expansion" of ϕ and the expressions obtained by substituting (27) and (28) in (16) and (20) are the "BI–RME representations" of ψ and $\nabla^2 \psi$; in fact, they consist of Boundary Integrals and Resonant Mode Expansions.

D. Discretization

The resonant mode expansions are approximated retaining the first M terms. Due to the smoothness of ϕ, it is expected that a reasonably small number of modes will be sufficient to represent the lowest-order eigenfunctions of the enlarged problem with good accuracy. On the other hand the part of the eigenvalue spectrum that must be calculated accurately must extend above $k_{\max}$, in order to evaluate the relevant terms of the pole expansion (2) with adequate precision. Therefore, by denoting the largest resonant wavenumber of the retained modes with $\lambda_{\max}$, the number M is chosen in such a way as to have

$$\lambda_{\max} \geq \zeta k_{\max} \tag{32}$$

where ζ is a parameter larger than one. The smallest allowed value of ζ has to be determined experimentally (see Section III). After truncation (27) and (28) can be written as

$$\phi = \mathbf{\Phi}^t \mathbf{a} \tag{33}$$

$$\nabla^2 \phi = -\mathbf{\Phi}^t \mathbf{\Lambda}^2 \mathbf{a} \tag{34}$$

where $\mathbf{\Phi}$ and $\mathbf{a}$ are M-dimensional vectors including the functions Φ_{pq} and amplitudes a_{pq} pertaining to the retained modes, $\mathbf{\Lambda}$ is the diagonal matrix consisting of the corresponding wavenumbers λ_{pq} and the superscript t denotes the transpose. Due to the orthogonality and the normalization of the Φ_{pq} we have

$$\langle \mathbf{\Phi}, \mathbf{\Phi}^t \rangle_\Omega = \mathbf{I} \tag{35}$$

where $\mathbf{I}$ is the $M \times M$ unit matrix and the brackets represent the inner product of $\mathcal{L}_2(\Omega)$.

The unknown function f is approximated by

$$f = \sum_{k=1}^{K} c_k w_k(s) + \sum_{p=1}^{P} b_p u_p(s)$$

where $\{w_k\}$ is a set of window functions ($w_k = 1$ in σ_k and zero elsewhere); $\{u_p\}$ is a set of subsectional basis functions, with support included in either element σ_k, and with *zero mean-value*; c_k and b_p are unknown coefficients. In matrix form we can write

$$f = \mathbf{w}^t \mathbf{c} + \mathbf{u}^t \mathbf{b} \tag{36}$$

where the vectors $\mathbf{w}$, $\mathbf{u}$ include the functions w_k, u_p and the vectors $\mathbf{c}$, $\mathbf{b}$ include the unknowns c_k and b_p.

Equations (24) and (25) are discretized using Galerkin's method, i.e., testing the first equation by the functions Φ_{pq} and the second by the functions u_p and w_k. Due to (35), considering the eigenfunction expansion of F_1 (see Appendix A), from (24) we obtain

$$-\mathbf{\Lambda}^2 \mathbf{a} + \chi^2 [\mathbf{a} + \mathbf{\Lambda}^{-4} (\mathbf{R}\mathbf{b} + \mathbf{S}\mathbf{c})] = 0, \tag{37}$$

where

$$\mathbf{R} = \int_\sigma \frac{\partial \mathbf{\Phi}}{\partial n} \mathbf{u}^t \, ds \tag{38}$$

$$\mathbf{S} = \int_\sigma \frac{\partial \mathbf{\Phi}}{\partial n} \mathbf{w}^t \, ds. \tag{39}$$

Testing (25), we obtain

$$\mathbf{C}\mathbf{b} + \chi^2 (\mathbf{R}^t \mathbf{a} - \mathbf{L}\mathbf{b} - \mathbf{T}\mathbf{c}) = 0 \tag{40}$$

$$\chi^2 (\mathbf{S}^t \mathbf{a} - \mathbf{T}^t \mathbf{b} - \mathbf{W}\mathbf{c}) = 0 \tag{41}$$

where

$$\mathbf{C} = \int_\sigma \int_\sigma G(s, s') \frac{\partial \mathbf{u}(s)}{\partial s} \frac{\partial \mathbf{u}^t(s')}{\partial s'} \, ds \, ds' \tag{42}$$

$$\mathbf{L} = \int_\sigma \int_\sigma \frac{\partial^2 F_1(s, s')}{\partial n \, \partial n'} \mathbf{u}(s) \, \mathbf{u}^t(s') \, ds \, ds' \tag{43}$$

$$\mathbf{T} = \int_\sigma \int_\sigma \frac{\partial^2 F_1(s, s')}{\partial n \, \partial n'} \mathbf{u}(s) \, \mathbf{w}^t(s') \, ds \, ds' \tag{44}$$

$$\mathbf{W} = \int_\sigma \int_\sigma \frac{\partial^2 F_1(s, s')}{\partial n \, \partial n'} \mathbf{w}(s) \, \mathbf{w}^t(s') \, ds \, ds' \tag{45}$$

(the expression of $\mathbf{C}$ is obtained integrating by parts with respect to s and observing that the σ_k are either closed lines or open lines with extremes on $\partial\Omega$, where $G = 0$).

Equations (37), (40), and (41) are satisfied identically by $\chi = 0$, $\mathbf{a} = 0$, $\mathbf{b} = 0$, and by any vector $\mathbf{c}$. These solutions correspond to the spurious ones discussed at the end of Section

II-B. As already stated, they are removed by the assumption $\chi \neq 0$. With this assumption (41) implies

$$\mathbf{c} = \mathbf{W}^{-1}(\mathbf{S}^t\mathbf{a} - \mathbf{T}^t\mathbf{b}). \tag{46}$$

The matrix $\mathbf{W}^{-1}$ can be deduced directly from the areas $S, S_1, S_2, \cdots, S_K$ shown in Fig. 2; in fact we have (see Appendix C)

$$(\mathbf{W}^{-1})_{hk} = \frac{\delta_{hk}}{S_k} + \frac{1}{S} \quad h, k = 1, \cdots, K. \tag{47}$$

Eliminating $\mathbf{c}$ from (37) and (40), we finally obtain

$$\begin{pmatrix} \mathbf{\Lambda}^6 & 0 \\ 0 & \mathbf{C} \end{pmatrix} \begin{pmatrix} \mathbf{a} \\ \mathbf{b} \end{pmatrix} = \chi^2 \begin{pmatrix} \mathbf{A} & \mathbf{D} \\ \mathbf{D}^t & \mathbf{B} \end{pmatrix} \begin{pmatrix} \mathbf{a} \\ \mathbf{b} \end{pmatrix} \tag{48}$$

where

$$\mathbf{A} = \mathbf{\Lambda}^4 - \mathbf{S}\mathbf{W}^{-1}\mathbf{S}^t$$
$$\mathbf{B} = \mathbf{L} - \mathbf{T}\mathbf{W}^{-1}\mathbf{T}^t$$
$$\mathbf{D} = \mathbf{S}\mathbf{W}^{-1}\mathbf{T}^t - \mathbf{R}$$

The matrices on both sides of (48) are symmetric and the one on the left-hand side is positive definite, due to the positive definiteness of $\mathbf{C}$ (see Appendix D). Then (48) has $M+P$ real eigenvalues and eigenvectors, which can be determined using very efficient and reliable library routines [7]. Furthermore, it is easily verified that the normalizing condition (26) is fulfilled if the eigenvectors satisfy

$$\mathbf{a}^t\mathbf{\Lambda}^6\mathbf{a} + \mathbf{b}^t\mathbf{C}\mathbf{b} = \chi^2. \tag{49}$$

It is expected that the smallest eigenvalues (that correspond to the most slowly-varying eigenfunctions ϕ) are the most accurate approximations for the eigenvalues of (24) and (25); in fact, (33) approximates ϕ by a band-limited function, so that the approximation is the better the smaller χ in comparison with $\lambda_{\max}$. For the same reason, the solutions with $\chi > \lambda_{\max}$ are meaningless.

E. Selection of the Internal Modes

Let χ, $\mathbf{a}$, $\mathbf{b}$ denote a solution of (48). From (20) and (34) we obtain

$$\nabla^2\psi^{\pm} = \chi^2\left[\pm\frac{f(s)}{2} + \int_\sigma \frac{\partial F_0(s, s')}{\partial n'} f(s')\, ds' - \mathbf{\Phi}^t\mathbf{\Lambda}^2\mathbf{a}\right]$$

where $\mathbf{\Phi}$ is taken on σ at the coordinate s; f is obtained from (36) and (46); the principal-value integral originates from the fact that "double-layer potential" U_0 [defined in (16)] is evaluated at σ. The internal solutions are identified by computing the norms

$$h^+ = ||\nabla^2\psi^+||_\sigma$$
$$h^- = ||\nabla^2\psi^-||_\sigma$$

and by checking the condition $h^- \gg h^+$; in fact, in these solutions $\nabla^2\psi^+$ is nominally zero (for details see [1], Section II-C).

Inaccurate solutions that cannot be clearly classified as either internal or external are likely to occur in the range of eigenvalues close to $\lambda_{\max}$. Increasing the number of the basis functions u_p and the number of the resonant modes [i.e., the coefficient ζ in (32)], the accuracy is increased and the range of inaccurate eigenvalues can be pushed well-above $k_{\max}$.

F. Calculation of c_{ni}

Let χ_i, $\mathbf{a}^{(i)}$, $\mathbf{b}^{(i)}$ correspond to the ith internal solution of the enlarged problem, i.e., to the eigenfunction ψ_i appearing in (4). From (15) and (20) we obtain

$$\nabla^2\psi_i = \begin{cases} -\chi_i^2 f_i & \text{on } \sigma \\ \chi_i^2\left[\displaystyle\int_\sigma \frac{\partial F_0(s, s')}{\partial n'} f_i(s')\, ds' - \mathbf{\Phi}^t\mathbf{\Lambda}^2\mathbf{a}^{(i)}\right] & \text{on } \partial\Omega \end{cases}$$

where

$$f_i = \mathbf{w}^t\mathbf{c}^{(i)} + \mathbf{u}^t\mathbf{b}^{(i)} \tag{50}$$

and $\mathbf{c}^{(i)}$ is obtained from (46). Therefore we have

$$c_{ni} = \begin{cases} \dfrac{-\chi_i[H_n c_k^{(i)} + \mathbf{p}_n^t\mathbf{b}^{(i)}]}{\kappa_i\sqrt{H_n}} & \text{if } \Sigma_n \in \sigma \\ \dfrac{\chi_i[\mathbf{v}_n^t\mathbf{c}^{(i)} + \mathbf{q}_n^t\mathbf{b}^{(i)} - \mathbf{r}_n^t\mathbf{\Lambda}^2\mathbf{a}^{(i)}]}{\kappa_i\sqrt{H_n}} & \text{if } \Sigma_n \in \partial\Omega \end{cases} \tag{51}$$

where we introduced the row-vectors

$$\mathbf{p}_n^t = \int_{\Sigma_n} \mathbf{u}^t\, ds$$
$$\mathbf{q}_n^t = \int_{\Sigma_n} ds \int_\sigma \frac{\partial F_0(s, s')}{\partial n'} \mathbf{u}^t(s')\, ds'$$
$$\mathbf{r}_n^t = \int_{\Sigma_n} \mathbf{\Phi}^t\, ds$$
$$\mathbf{v}_n^t = \int_{\Sigma_n} ds \int_\sigma \frac{\partial F_0(s, s')}{\partial n'} \mathbf{w}^t(s')\, ds'$$
$$= -\frac{H_n}{ab} \quad (S_1, S_2, \cdots, S_K)$$

(the last equality is demonstrated in Appendix C).

III. Effect of a Deformation of σ

A deformation of σ perturbs the eigenvalues and the eigenfunctions of (5) and changes the frequency response of the component, due to the perturbation of the poles and the residues of the Y-parameters. Evaluating the effect of a slight deformation is important both for setting the mechanical tolerances and for including the algorithm in a CAD tool performing the optimization of the response by subsequent deformations of σ.

Let us consider a perturbation which displaces a generic point $\vec{r}$ along the normal $\vec{n}$ from a smooth part of σ to a new position

$$\vec{r}(s) - \nu\Theta(s)\,\vec{n}(s)$$

where ν is a small parameter and Θ is a continuous function. Due to perturbation, the quantities κ_i, c_{ni} assume new values $\tilde{\kappa}_i$, $\tilde{c}_{ni}$, that are obtained from (4) and (8) by replacing χ_i

and ψ_i with the corresponding perturbed quantities. These quantities can be obtained from the perturbation formulas (9.2.52), (9.2.53) given in [8]. After some manipulations, not reported for reasons of space, we obtain

$$\tilde{\kappa}_i^2 = \kappa_i^2 + \nu\,\chi_i^2(q_{ii} - p_{ii}) + O(\nu^2) \tag{52}$$

$$\tilde{c}_{ni} = Q_i^{-(1/2)} \sum_j \alpha_{ij}\, c_{nj} + O(\nu^2) \tag{53}$$

where

$$q_{ij} = \int_\sigma \Theta \psi_i \psi_j \, d\sigma \tag{54}$$

$$p_{ij} = \frac{1}{\chi_i \chi_j} \int_\sigma \Theta \frac{\partial \psi_i}{\partial s} \frac{\partial \psi_j}{\partial s} \, d\sigma$$

$$\alpha_{ii} = 1$$

$$\alpha_{ij} = \nu \frac{\chi_i^2 q_{ij} - \chi_i \chi_j p_{ij}}{\chi_i^2 - \chi_j^2} \quad (i \neq j)$$

$$Q_i = \sum_j \alpha_{ij}^2 - \nu \sum_{p,q} \alpha_{ip} \alpha_{iq} q_{pq} \tag{55}$$

On the other hand, due to (13), ψ can be replaced by f in (54) and (55) (remember that $\psi^+ = 0$ in internal solutions). Then, using (50) we obtain

$$q_{ij} = \mathbf{b}^{(i)t} \mathbf{X}\, \mathbf{b}^{(j)} + \mathbf{b}^{(i)t} \mathbf{Y}\, \mathbf{c}^{(j)} + \mathbf{b}^{(j)t} \mathbf{Y}\, \mathbf{c}^{(i)} + \mathbf{c}^{(i)t} \mathbf{Z}\, \mathbf{c}^{(j)}$$

$$p_{ij} = \frac{\mathbf{b}^{(i)t} \mathbf{X}'\, \mathbf{b}^{(j)}}{\chi_i \chi_j}$$

where we introduced the matrices

$$\mathbf{X} = \int_\sigma \Theta\, \mathbf{u}\mathbf{u}^t \, ds \tag{56}$$

$$\mathbf{X}' = \int_\sigma \Theta \frac{\partial \mathbf{u}}{\partial s} \frac{\partial \mathbf{u}^t}{\partial s} \, ds \tag{57}$$

$$\mathbf{Y} = \int_\sigma \Theta\, \mathbf{u}\mathbf{w}^t \, ds \tag{58}$$

$$\mathbf{Z} = \int_\sigma \Theta\, \mathbf{w}\mathbf{w}^t \, ds \tag{59}$$

The calculation of these matrices is trivial, so that the extra computational work required for evaluating the effect of a perturbation is negligible.

IV. Implementation and Testing of the Algorithm

The boundary σ is approximated by one or more polygonals, whose sides are subdivided into segments no longer than $\pi/(2\lambda_{\max})$. The basis functions u_p are zero-mean piece-wise parabolic splines defined over four adjacent segments (see Fig. 3). As shown in the same figure, special functions defined over only three segments are used at the extremes of the lines σ_k that touch $\partial\Omega$. A denser segmentation is used near the edges, to better approximate the rapid variations of f. Note that the number of the segments increases with $\lambda_{\max}$, so that increasing the parameter ζ not only increases the number of resonant modes [see (32)] but also the number of basis functions. For this reason, the value of ζ is expected to determine the accuracy of the calculation.

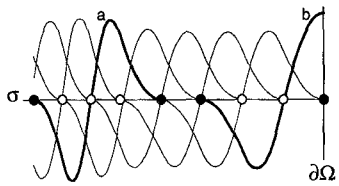

Fig. 3. Zero-mean piece-wise parabolic splines used as basis functions. a is a function defined over four segments and b is a special function defined at an extreme of σ.

In the calculation of the matrices **C**, **L**, **T**, **R**, **S** we evaluate all integrals using Gauss quadrature formulas, except for the entries of **C**, **L**, **T** that involve overlapping basis functions. As usual in the boundary element method, in these cases we evaluate the contributions from the singularities of the Green's functions analytically, and the contributions from their regular parts numerically.

Once the matrices **A**, **B**, **D** have been formed, the eigenvalue equation (48) is solved using LAPACK routines [7]. Then the selection of the internal modes is performed, calculating the norms h^+ and h^- as discussed in [1].

After the resonant wavenumbers κ_i and the coefficients c_{ni} have been calculated, the values of the Y-parameters are evaluated by (2) at many frequencies in the operating band of the waveguides and the S-parameters are deduced from them.

It is noted that in cases of structures with one or two symmetry planes the algorithm for the mode calculation can be modified to take advantage of the symmetry. This modification is not discussed for brevity.

As in the case of H-plane components [1], we tested the algorithm using a simple waveguide section as a benchmark. In particular, the test permitted us to find the effect of the choice of the parameter ζ in (32). We verified that the accuracy increases with increasing ζ, that demonstrates the convergence of the algorithm. Furthermore, we observed that the accuracy was acceptable from values of ζ as low as 2.5. On the other hand, since the CPU time increases rapidly with ζ, a good trade-off between accuracy and time is to choose ζ in the range 2.5–4. Note that this range is the same as that considered in the H-plane case [1].

The algorithm described in this paper and the one described in [1] were implemented in a computer code, named ANAPLAN-W [9].

V. Examples and Comparison with the Finite Element Method

We report the results of some calculations to validate the algorithm and to show how it can be used in the design of components of practical interest, obtaining a very good accuracy with a short computing time (the reported CPU times refer to a SUN SparcStation 10).

Fig. 4 refers to a 90° mitered E-bend, in the case of a diagonal mitering ($d/b = 0.707$) and in the limiting case of no miter ($d/b = 1.41$). Using $\zeta = 2.5$, the frequency response over the whole band was obtained in 3.1 s and 2.3 s, in the

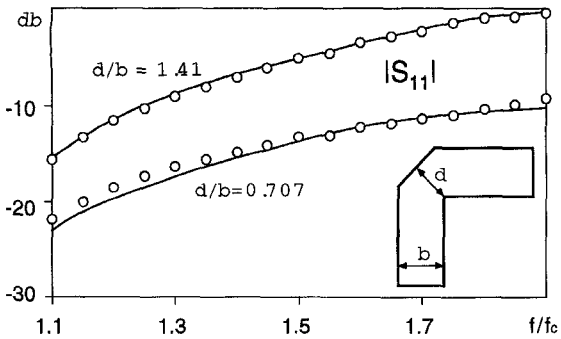

Fig. 4. Normalized frequency response of a mitered E-plane 90° bend. Solid lines, this method; circles, computed values from [10].

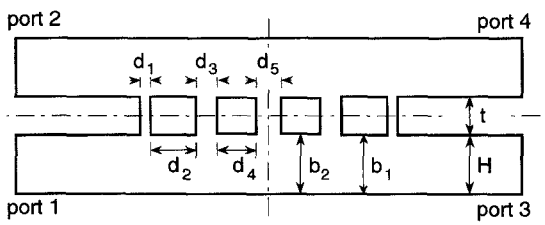

Fig. 5. Geometry of the 4-*db* coupler in WR-75 waveguide considered in [11]. The dimensions (in mm) are: $H = 9.52$; $t = 6.16$; $b_1 = 9.52$; $b_2 = 9.72$; $d_1 = 1.7$; $d_2 = 7.34$; $d_3 = 3.4$; $d_4 = 6.26$; and $d_5 = 4.53$. The width of the waveguides is $W = 19.05$ mm.

two cases, respectively. Our results compare very well with the mode-matching results reported in [10].

The second example refers to the 4-*db* branch-guide coupler of Fig. 5. The dimensions (see caption) were taken from [11]. Fig. 6 shows an excellent agreement between our results and those reported in [11]. Considering the double reflection symmetry and using $\zeta = 3.5$, the CPU time was only 56 s for the complete frequency response.

The last example concerns the analysis of the rat-race directional coupler (see Fig. 7) recently considered in [12]. Fig. 8 shows an excellent agreement between our results and those reported in [12], obtained by the boundary contour mode matching method. The experimental results reported in the same figure differ slightly from the computed ones, presumably due to losses. Using $\zeta = 3.5$ and exploiting the reflection symmetry, the calculation of the complete frequency response required 195 s. It is noted that in this example the CPU time was longer than in the previous ones. The reason is that no part of the boundary fits with $\partial\Omega$, so that σ coincides with the whole boundary and a large number of basis functions must be considered.

The eigenvalue problem (5) could be solved by many different algorithms, the most classical one being the finite element method (FEM) [13]. For this reason, we carried out many calculations using both the FEM and the BI–RME method, to check the practical advantage of our approach. To minimize the CPU time, in each calculation the refinement of the FEM mesh was just sufficient to obtain an accuracy comparable to that of our method, and symmetries were exploited, whenever possible. Furthermore, the sparsity of the FEM matrices was exploited using the Lanczos' algorithm [14] to solve the eigenvalue problem.

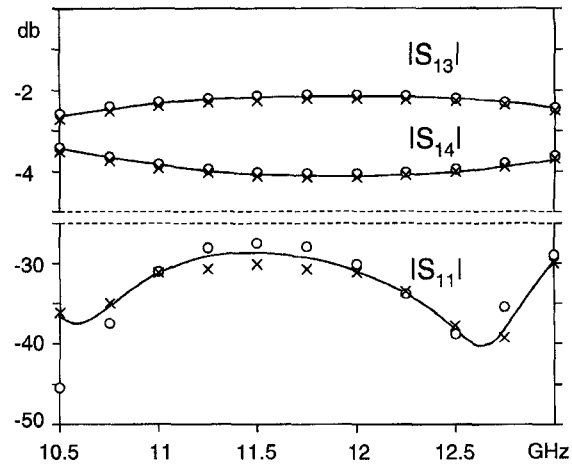

Fig. 6. Scattering parameters of the coupler of Fig. 5. Solid lines, this method; crosses, computed values from [11]; and circles, measured values from [11].

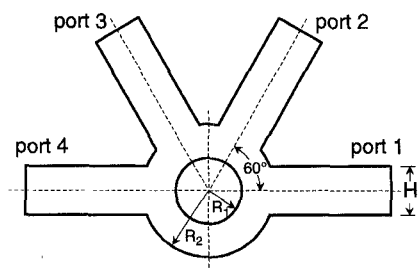

Fig. 7. Cross section of the E-plane rat-race 3-*db* directional coupler considered in [12]. The dimensions (in mm) are: $H = 7.9$; $R_1 = 5.35$; and $R_2 = 10.875$. The width of the waveguides is $W = 15.799$.

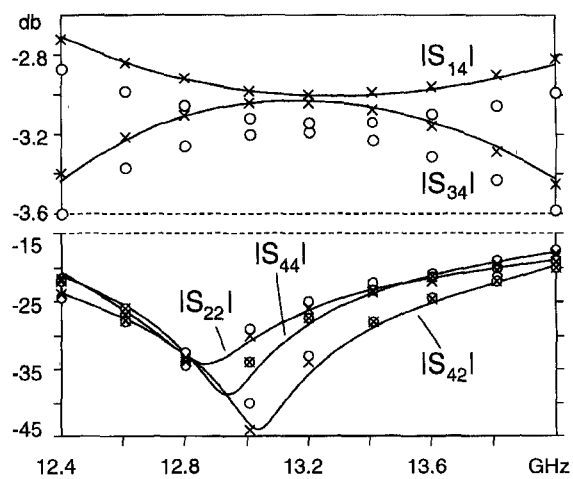

Fig. 8. Scattering parameters of the rat-race of Fig. 7. Solid lines, this method; crosses, computed values from [12]; and circles, measured values from [12].

Though, in some cases, we found that the two methods required comparable times, in many cases, the use of the BI–RME method resulted in a typical time saving of one order of magnitude. The loss of efficiency of the Lanczos' algorithm was not related to the complexity of the component, but, seemingly, to the presence of clusters of eigenvalues. Note that these clusters are likely encountered in the analysis of

practical components (e.g., filters with closely spaced poles). Incidentally, clustered eigenvalues do not create troubles if the eigenvalue problem is solved by the procedure described in [13]; the CPU time, however, increases dramatically. For instance, in the analysis of the coupler of Fig. 5, which required the calculation of about 150 eigensolutions, the CPU-time (referred to a SUN SparcStation 10) was 100 min with the FEM, exceeding by two orders of magnitude the BI–RME CPU-time. In conclusion, solving the eigenvalue problem by our method rather than by the FEM is normally very convenient.

The FEM is also used in commercial e.m. solvers, e.g., HFSS [15]. Of course, the advantage of our specialized method over general purpose e.m. solvers is out of question. For instance, the time required by our code ANAPLAN-W for the calculation of the *whole* frequency response reported in Fig. 6 was about 1/6 of the time required by HFSS for calculating the S-parameters at a *single* frequency.

VI. Conclusion

The reported theory is a bit complicated, but it results in a very efficient algorithm for the wideband analysis of E-plane components. The efficiency depends on the possibility of determining the poles and the residues of the Y-parameters by the solution of a linear matrix eigenvalue problem, involving matrices of reasonably small order. The reported examples demonstrate that the wideband modeling of complicated structures can be carried out in times shorter by more than one order of magnitude, compared to those required by standard FEM software.

Either for its rapidity and for the possibility of a quick evaluation of the effect of a deformation on the frequency response, the method is ideally suited for use in a CAD code, together with an optimization routine. Using a standard workstation, optimized design requiring many tens or hundreds of subsequent analyses can be obtained in reasonable times. This justifies the effort to write a new BI–RME based code, instead of merely using a standard e.m. solver.

Appendix A
Deduction of (18) and Eigenfunction Expansions of the Green's Functions

Let us consider the vectors

$$\vec{e}_{pq}^{\,\mathrm{TE}} = \frac{\vec{u}_z \times \nabla \Phi_{pq}}{\lambda_{pq}}$$
$$\vec{e}_{pq}^{\,\mathrm{TM}} = -\frac{\nabla \Psi_{pq}}{\mu_{pq}}$$

where Φ_{pq}, λ_{pq} are given by (29), (30) and

$$\Psi_{pq} = \sqrt{\frac{2}{ab}} \sin\frac{p\pi x}{a} \sin\frac{q\pi y}{b}$$
$$\mu_{pq} = \sqrt{\left(\frac{p\pi}{a}\right)^2 + \left(\frac{q\pi}{b}\right)^2} \qquad p, q = 1, 2, \cdots$$

It is well known that these vectors constitute a complete orthonormal basis for representing any square-integrable vector field defined in Ω. This implies the "completeness relationship"

$$\sum_{p,q} \vec{e}_{pq}^{\,\mathrm{TE}}(\vec{r})\, \vec{e}_{pq}^{\,\mathrm{TE}}(\vec{r}') + \sum_{p,q} \vec{e}_{pq}^{\,\mathrm{TM}}(\vec{r})\, \vec{e}_{pq}^{\,\mathrm{TM}}(\vec{r}') = \overleftrightarrow{1}\, \delta(\vec{r} - \vec{r}')$$

where $\overleftrightarrow{1}$ denotes the unit dyadic and $\vec{r}$, $\vec{r}'$ are points of Ω. From this equation we obtain

$$\vec{u}_z \times \nabla\nabla' \underbrace{\sum_{p,q} \frac{\Phi_{pq}(\vec{r})\Phi_{pq}(\vec{r}')}{\lambda_{pq}^2}}_{F_0} \times \vec{u}_z = \nabla\nabla' \underbrace{\sum_{p,q} \frac{\Psi_{pq}(\vec{r})\Psi_{pq}(\vec{r}')}{\mu_{pq}^2}}_{G} \qquad \vec{r} \neq \vec{r}' \tag{A1}$$

where the series are identified with F_0 and G, because they are the solutions of (17) and (22) in the form of eigenfunction expansions. Then we can also write $\nabla\nabla' F_0 = \vec{u}_z \times \nabla\nabla' G \times \vec{u}_z$ and, therefore, placing the source point at the point s' of σ

$$\nabla \frac{\partial F_0(\vec{r}, s')}{\partial n'} = \vec{u}_z \times \nabla\nabla' G(\vec{r}, s') \cdot \vec{u}_z \times \vec{n}' = \vec{u}_z \times \nabla \frac{\partial G(\vec{r}, s')}{\partial s'}$$

Then, looking at the definition (16) of U_0, we have

$$\nabla U_0(\vec{r}) = \vec{u}_z \times \nabla \int_\sigma \frac{\partial G(\vec{r}, s')}{\partial s'} f(s')\, ds' = -\vec{u}_z \times \nabla \int_\sigma G(\vec{r}, s') \frac{\partial f(s')}{\partial s'}\, ds' \quad (\vec{r} \notin \sigma) \tag{A2}$$

Finally, (21) is obtained from (A2) allowing $\vec{r}$ to tend to the point s of σ and taking the normal component of both sides.

It is also noted that, according to (18), the eigenfunction expansion of F_1 is

$$F_1 = \sum_{p,q} \frac{\Phi_{pq}(\vec{r})\Phi_{pq}(\vec{r}')}{\lambda_{pq}^4}$$

Appendix B
Normalization of ϕ and f

Equation (9) implies (and is implied by)

$$\psi = -\chi^{-2}\nabla^2\psi = \chi^{-4}\nabla^2\nabla^2\psi$$

Therefore, the normalizing condition (11) is equivalent to

$$-\langle \nabla^2\psi, \nabla^2\nabla^2\psi \rangle_\Omega = \chi^6$$

where $\langle , \rangle_\Omega$ denotes the inner product of $\mathcal{L}_2(\Omega)$. Furthermore,

due to (20) and because $\nabla^2 U_0 = 0$ in $\Omega^\dagger$, we have

$$-\langle \nabla^2\phi + U_0,\, \nabla^2\nabla^2\phi\rangle_\Omega = \chi^2$$

This equation is converted into (26) observing that, due to the Neumann boundary conditions satisfied on $\partial\Omega$ by U_0, and $\nabla^2\phi$ and due to the continuity of $\nabla^2\phi$, $\partial\nabla^2\phi/\partial n$ and $\partial U_0/\partial n$ on σ, we have

$$\begin{aligned}
-\langle \nabla^2\phi, \nabla^2\nabla^2\phi\rangle_\Omega &= \int_\Omega |\nabla\nabla^2\phi|^2 d\Omega \\
-\langle U_0, \nabla^2\nabla^2\phi\rangle_\Omega &= \int_\sigma (U_0^- - U_0^+)\,\frac{\partial\nabla^2\phi}{\partial n}\,ds \\
&= \int_\sigma f(s)\,\frac{\partial\nabla^2\phi}{\partial n}\,ds
\end{aligned}$$

The last integral is converted into the double integral in (26) substituting the expression of $\nabla^2\phi$ obtained from (24), using (25) and integrating by parts with respect to s.

Appendix C
Expressions of $\mathbf{W}^{-1}$ and $\mathbf{v}_n$

From (45) we have

$$\begin{aligned}
W_{hk} &= \int_{\sigma_h} ds\,\frac{\partial}{\partial n}\int_{\sigma_k}\frac{\partial F_1}{\partial n'}\,ds' \\
&= -\int_{\sigma_h} ds\,\frac{\partial}{\partial n}\int_{S_k}\nabla'^2 F_1(\vec{r},\vec{r}')\,dS_k' \\
&= \int_{\sigma_h} ds\,\frac{\partial}{\partial n}\int_{S_k} F_0(\vec{r},\vec{r}')\,dS_k' \\
&= \int_{S_k} dS_k'\int_{\sigma_h}\frac{\partial F_0(\vec{r},\vec{r}')}{\partial n}\,ds \\
&= -\int_{S_k} dS_k'\int_{S_h}\nabla^2 F_0(\vec{r},\vec{r}')\,dS_h \\
&= \int_{S_k}\int_{S_h}\left[\delta(\vec{r}-\vec{r}') - \frac{1}{ab}\right] dS_k'\,dS_h \\
&= S_h\,\delta_{hk} - \frac{S_h S_k}{ab}
\end{aligned}$$

Due to the particular form of $\mathbf{W}$, the inverse can be obtained by the Sherman–Morrison formula [16]. The result is (47).

The kth element of the vector $\mathbf{v}_n$ is

$$\begin{aligned}
\int_{\Sigma_n} ds\int_{\sigma_k}\frac{\partial F_0}{\partial n'}\,ds' &= -\int_{\Sigma_n} ds\int_{S_k}\nabla'^2 F_0(\vec{r},\vec{r}')\,dS_k' \\
&= -\int_{\Sigma_n} ds\int_{S_k}\frac{1}{ab}\,dS_k' \\
&= -\frac{H_n S_k}{ab}
\end{aligned}$$

because $\vec{r}\in\Sigma_n$ is outside of S_k.

Appendix D
Positive Definiteness of the Matrix C

Substituting the eigenfunction expansion of G [see (A1)] in (42), we immediately obtain

$$\sum_{i=1}^{P}\sum_{j=1}^{P} C_{ij} b_i b_j = \sum_{p,q}\left(\sum_{i=1}^{P} b_i\int_\sigma \frac{\Phi_{pq}}{\lambda_{pq}}\,\frac{\partial u_i}{\partial s}\,ds\right)^2$$

which is positive for any $\mathbf{b}\neq 0$.

Acknowledgment

The authors would like to thank the Microwave Group of the Politecnico di Milano for their cooperation in the HFSS simulations. Also the Istituto di Analisi Numerica (CNR Pavia) for making available its FEM software and, in particular, Dr. C. Chinosi, Prof. L. Gastaldi, and Dr. V. Simoncini for their suggestions and assistance in the production of the FEM results.

References

[1] G. Conciauro, P. Arcioni, M. Bressan, and L. Perregrini, "Wideband modeling of arbitrarily shaped H-plane components by the boundary integral–resonant mode expansion method," *IEEE Trans. Microwave Theory Tech.*, vol. 44, no. 7, pp. 1057–1066, July 1996.

[2] M. Bressan, G. Conciauro, and P. Gamba, "Analysis of guided modes in multilayer/multiconductor structures by the boundary integral–resonant mode expansion method," *IEEE Trans. Microwave Theory Tech.*, vol. 44, no. 5, pp. 659–667, May 1996.

[3] G. Conciauro, M. Bressan, and C. Zuffada, "Waveguide modes via an integral equation leading to a linear matrix eigenvalue problem," *IEEE Trans. Microwave Theory Tech.*, vol. MTT-32, no. 11, pp. 1495–1504, Nov. 1984.

[4] P. Arcioni, M. Bressan, and G. Conciauro, "A new algorithm for the wideband analysis of arbitrarily shaped planar circuits," *IEEE Trans. Microwave Theory Tech.*, vol. 36, no. 10, pp. 1426–1437, Oct. 1988.

[5] P. Arcioni, M. Bressan, and L. Perregrini, "A new boundary integral approach to the determination of the resonant modes of arbitrarily shaped cavities," *IEEE Trans. Microwave Theory Tech.*, vol. 43, no. 8, pp. 1848–1856, Aug. 1995.

[6] G. Conciauro, L. Perregrini, and P. Belloni, "Wideband analysis of E-plane metal insert filters by the boundary integral–resonant mode expansion method," in *Proc. 25th European Microwave Conf.*, Bologna, Sept. 4–7, 1995, pp. 742–745.

[7] E. Anderson *et al.*, *LAPACK, User's Guide.* Philadelphia: SIAM, 1992.

[8] P. M. Morse and H. Feshbach, *Methods of Theoretical Physics.* Kogakusha, Tokyo: McGraw-Hill, 1953.

[9] P. Arcioni, M. Bressan, L. Perregrini, G. Conciauro, and G. Gatti "ANAPLAN-W: A CAD tool for E/H-plane waveguide circuits," *ESA—Preparing for the Future*, vol. 6, no. 1, pp. 12–13, Mar. 1996.

[10] F. Alessandri, M. Mongiardo, and R. Sorrentino, "Rigorous mode matching analysis of mitered E-plane bends in rectangular waveguide," *IEEE Microwave Guided Wave Lett.*, vol. 4, no. 12, pp. 408–410, Dec. 1994.

[11] F. Alessandri, G. Bartolucci, and R. Sorrentino, "Admittance matrix formulation of waveguide discontinuity problems: Computer aided design of branch guide directional couplers," *IEEE Trans. Microwave Theory Tech.*, vol. 36, pp. 394–403, Feb. 1988.

[12] J. M. Reiter and F. Arndt, "Rigorous analysis of arbitrarily shaped H- and E-planes discontinuities in rectangular waveguides by a full-wave boundary contour mode-matching method," *IEEE Trans. Microwave Theory Tech.*, vol. 43, no. 4, pp. 796–801, Apr. 1995.

[13] P. Silvester, "A general high-order finite-element waveguide analysis program," *IEEE Trans. Microwave Theory Tech.*, vol. 17, no. 4, pp. 204–210, Apr. 1969.

[14] M. T. Jones and M. L. Patrick, "LANZ: Software for solving the large sparse symmetric generalized eigenproblem," *NETLIB On-Line Documentation*, http://www.netlib.org/lanz/index.html.

[15] Hewlett-Packard Co., 1421 S. Manhattan Ave., Fullerton, CA 92631, (714)758-5497.

[16] G. Dahlquist and A. Bjorck, *Numerical Methods.* Englewood Cliffs, NJ: Prentice-Hall, 1969, p. 161.

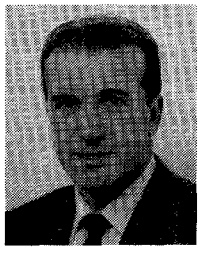

Paolo Arcioni (M'95) was born in Busto Arsizio, Italy, in 1949. He received the degree in electronic engineering from the University of Pavia, Italy, in 1973.

He joined the Department of Electronics of the University of Pavia as a Researcher in electromagnetics and has been teaching a course in Microwave Theory as an Associate Professor since 1976. His current research interest concerns the development of numerical methods for the electromagnetic CAD of passive microwave components and of interaction structures for particle accelerators. In 1990, he spent a period as Visiting Scientist at the Stanford Linear Accelerator Center, CA, where he was involved with the RF group in the design of optimized cavities for the PEP II project.

Mr. Arcioni is a member of the AEI.

Marco Bressan (M'93) was born in Venice, Italy, in 1949. He received the degree in electronic engineering from the University of Pavia in 1972.

Since 1973, he has been with the Department of Electronics of the University of Pavia, as a Researcher in the field of electromagnetics. In 1987, he joined the Faculty of Engineering of the University of Pavia, where currently he teaches a course on Antennas and Propagation as an Associate Professor. His main research interests are in antenna theory and in analytical and numerical techniques for electromagnetics.

Mr. Bressan is a member of the Editorial Board of the IEEE TRANSACTIONS ON MICROWAVE THEORY AND TECHNIQUES.

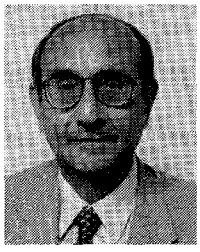

Giuseppe Conciauro (A'72–M'93) was born in Palermo, Italy, in 1937. He received the degree in electrical engineering from the University of Palermo, Italy in 1961 and the "Libera Docenza" in electronics in 1971.

From 1963 to 1971, he was with the Institute of Electrical Engineering of the University of Palermo as an Assistant Professor of microwave theory. In 1971, he joined the Department of Electronics of the University of Pavia, Italy, where he taught microwave theory as an Associate Professor, until 1980. Since that year, he has been teaching electromagnetic theory at the same University, as a Full Professor. From 1985 to 1991, he has served as Director of the Department of Electronics of the University of Pavia. His main research interests are in microwave theory, interaction structures for particle accelerators, and numerical methods in electromagnetics.

Dr. Conciauro is a member of AEI and of the Editorial Board of the IEEE TRANSACTIONS ON MICROWAVE THEORY AND TECHNIQUES.

Luca Perregrini was born in Sondrio, Italy, in 1964. He received the degree in electronic engineering and the Ph.D. degree from the University of Pavia in 1989 and 1993, respectively.

In 1992, he joined the Department of Electronics of the University of Pavia as a Researcher in electromagnetics. His current research interests are in numerical methods for the analysis and optimization of waveguide circuits.